# CONCRETE ICE ABRASION: DETERIORATION MECHANISMS, TESTING AND MODELING

S.Jacobsen[1], A.Bekker[2], T.Uvarova[2], E.Pomnikov[2], L.Kim[2] and K.T. Fosså[3]

[1]Norwegian University of Science and Technology, Trondheim, Norway
[2]Far Eastern Federal University, Vladivostok, Russia
[3]Kværner ASA, Snarøyveien 30, NO-1360 Fornebu, Norway

## ABSTRACT

Ice in mechanical contact with concrete structures in arctic and sub-arctic areas can cause severe abrasion from impact and sliding of sea ice. The concrete abrasion depths can be in the order of tens of mm over a couple of decades. Mechanisms causing the relatively weak ice to abrade the relatively stronger concrete are reviewed such as protruding aggregate loosening, low angle asperity yielding, hydraulic pressure, grit, scratching and percussion. A newly developed model from Far Eastern Federal University (FEFU) (Vladivostok, Russia) combining ice drift models, ice-structure impact modelling and laboratory ice abrasion tests was applied in investigation of concrete abrasion mechanisms. The complete laboratory test and modelling tool has been applied in the development of suitable ice abrasion resistant concrete for the Sea of Okhotsk. An effort was made in a separate study to estimate the contact area of ice impacts assuming that the concrete damage mechanism is from high pore-water pressure in the concrete surface due to short time indentation of the rough concrete surface into pure ice crystals. Due to the ice impact and sliding, water in the contact zone between ice and concrete can be pressed into the concrete at a contact pressure limited by hardness of ice crystals. By performing simulations with pressure equal to short time hardness of pure ice crystals it was found, when assuming pore water pressure as the only concrete fracture mechanism, that only around 0.15 % of the ice-concrete surface was deteriorated simultaneously in the process, if to arrive at same results as the newly developed model from FEFU mentioned above.

**Key-words:** concrete, durability, offshore, ice abrasion, lab test, numerical simulation, damage mechanism

## INTRODUCTION

Ice movement can cause severe abrasion on different concrete structures. Sea ice can move towards marine structures [1, 2] like bridges, piers, oil-platforms and sea wind mill foundations [3] or fresh water ice in reservoirs can act on the upside face of concrete dams, along canals, in rivers. Ice can also act in the pores of concrete as hydraulic pressure [4, 5], as a propagating ice front in a concrete frost test [6, 7] or due to different thermal expansion coefficients concrete-ice [8, 9]. This abrasion can affect the service life and precautions are therefore necessary when designing and producing concrete structures for the arctic. This paper presents experiences with ice abrasion modelling based on observations of sea ice conditions in the Sea of Okhotsk,

laboratory tests of ice abrasion and numerical modelling. Furthermore, a material fracture mechanism due to ice-concrete hydraulic contact pressure is proposed to proceed in the modelling and prediction of ice abrasion resistant concrete.

## BACKGROUND

On marine structures exposed to sea ice an average ice pressure $P_{ice}$ in the order of 1 MPa is common [1]. The local ice-structure contact pressure can be much higher; measured at ≈ 15 MPa due to crushing [10] and measured up to ≈ 42 MPa due to impact [11]. The rate of concrete ice abrasion can be several mm per year depending on concrete and ice conditions as observed in a number of studies reviewed in [12]. Field inspection has revealed that normal pressure and/or normal ice impact causes less abrasion compared to ice sliding along the surface [13, 14]. Figure 1 shows ice abrasion on a pier of the Canadian Confederation bridge [15].



*Figure 1 - 0.3 mm/yr ice abrasion on 90 MPa Confederation Bridge concrete after 8 years [15]*

Figure 1 shows that paste is the most abraded part of the surface whereas a number of coarse aggregate particles protrude as observed by Huovinen [1,2]. Apparently the aggregate is more ice abrasion resistant than cement paste as for other types of abrasion [16]. Tests on specimens of 30 – 60 MPa concrete mounted in the bow of an ice-breaker [1] showed 2 – 5 mm concrete abrasion depth after a few hours passing only 40 km length in the ice covered Baltic Sea, i.e. ice abrasion rate in the order of 0.1 mm/km ice passage. Thus, Huovinen's accelerated ice-breaker test showed that the ice-abrasion phenomenon can be regarded as an individual deteriorating mechanism. However, his model only considers sliding, mechanical properties and not the permeability which in most cases controls concrete durability. Steady state ice abrasion rate seems to prevail once the paste layer at the surface is abraded. This has been observed both in laboratory [12] and by comparing ice abrasion depth on a Finnish lighthouse after 26 and 44 years of exposure [1, 12, 17]. Sliding abrasion and impact abrasion seem to be two different modes of ice action on the concrete surface. In Huovinen's model pressure with impact/crushing and sliding, are imposed as normal and shear stresses. Some simplified formulae were derived from the numerical model expressing abrasion as function of strength and ice movement.

Other effects that can explain how a softer material can abrade a mechanically stronger one exist. Asperities in harder metals with top angle lower than a critical value may yield plastically as they plough a softer metal as shown both theoretically and experimentally in [18] (though steel is expected to protect against ice abrasion [19]). A three-phase abrasion mechanism may also work with a grit of crushed ice and concrete acting as the third phase between ice and concrete [20]. A

combination of scratching, fatigue and percussion-abrasive wear is proposed in [21] with the concrete abrasion in mm/(km·Pa) as a purely empirical rate determined in ice abrasion testing with controlled pressure and passage.

Ice hardness determined as effective stress (load/indented contact area) can be used to describe contact pressure. An early study of the Moh hardness of ice reported an increase with reducing temperature; from 2 near 0°C, 4 around -40°C to 6 around -50°C [22]. It was claimed that air-born ice particles can abrade even some igneous rocks. Hardness of pure ice crystals can be quite high [23] and depends on temperature, direction and loading rate: from 70 N/mm$^2$ on the prismatic plane 90° to the c-axis at – 12.5 0°C down to 27 N/mm$^2$ at -5 °C on the same plane 45° to the c-axis. Similar hardness was found in [24] varying somewhat with surface preparation and load level. Indenting measurements on sea ice with a steel ball [25] gave lower hardness than in pure crystals; around 15 N/mm$^2$ at -10°C. In concrete there can be several constituents with higher hardness than this [26], though also weak components with capillary porosity and Interfacial Transition Zones (ITZ). Therefore more research on mechanisms causing ice abrasion on concrete and development of abrasion models is needed. This could be a supplement to observations of real ice abrasion on structures and accelerated concrete ice abrasion laboratory tests. Hopefully it could enable complete modelling and service life prediction by ice drift-, environment- and concrete material data and -models.

**CONCRETE ICE ABRASION PREDICTIONS BY ICE DRIFT AND ABRASION TEST**

**Ice conditions and structure-ice impact calculation**

Research to predict the ice abrasion of concrete placed in the Sea of Okhotsk has to a large extent been based on detailed knowledge of local ice conditions. The average duration of the ice period in the oil and gas fields in the south-western part of the Sea of Okhotsk is 160-180 days. Ice formation begins in the end of November. Stable sheet ice appears in the end of December, ice with thickness exceeding 0.3 m appears in January. In March and early April the ice conditions are most complicated. Concentration of drifting ice is up to 9-10 points. Ice cakes (less than 20 m) appear throughout November – January in small quantities with occurrence probability of 5-7%. In February-March ice cakes are not observed, and re-appear in April with occurrence probability of 11%, in May-June the occurrence probability of ice cakes increases to 25% and more. Small ice (20-100 m) in the first half of the ice period comprises 20% of the occurrence probability, and in the second period 40%. Throughout January – April medium ice (100-500 m) generally prevails with occurrence probability often exceeding 50%. In December and May medium ice quantity decreases by 2-3 times. Occurrence of big ice floes (500-2000 m) might happen throughout January-May, but occurrence probability over 50% is observed only in particular decades of March. Vast ice fields (2-10 km) and giant ice fields (over 10km) may only be encountered from late January till mid April, and their occurrence probability never exceeds 10%. The overall length of ice fields shifting through the oil & gas field is an indirect indicator of ice regime severity in regard to loads on offshore structures. During each ice season, 306 km of ridged ice and 2138 km of level ice (at average) shift through the north-eastern offshore zone.

*Figure 2 – Concrete structures placed in the Sea of Okhotsk 2004 and 2005, Fosså [19]*

The general ice drift pattern is determined by prevailing winds, currents and tidal effects. The general drift direction (South – North-East) almost coincides with the Eastern Sakhalin current. The maximum velocities of Eastern Sakhalin current are observed in January-February. High drift velocities are determined by strong winds of dominant northern directions. Constant currents and tidal effects influence the ice drift considerably. Figure 2 shows two concrete structures that have now been in service in this area since 2004 and 2005.

Spatial variability of ice drifting in the north-east shelf of Sakhalin Island is characterized by speed decrease towards south. The maximum ice drift velocity observed varies from 2.5 m/s in Northern areas to less than 1.0 m/s in southern areas. In the oil and gas fields the drifting velocity is approximately 2.0 m/s. The highest drift velocities are those parallel to the coastline.
No ice floes of particular thickness prevail within Sakhalin island north-eastern offshore oil & gas production areas. Ice floes of 0.3-1.2 m thickness are most typically observed. In April one-year thin 0.3-0.7 m ice and one-year average thickness ice 0.7-1.2 m become dominant. Their coverage area is 40-50% and 30-40% respectively. One-year thick ice of 1.2 m and more, dominate in May covering 30-50% of the water area. In April-May ice of 0.7-1.2 m thickness is observed in 50% of the occurrences, 18% is more than 1.2 m thick and 26% is 0.3-0.7 m thick. Average thickness of ice throughout the season is 0.65 m. Ice formations of constant thickness exceeding 1.5 m offshore the Sakhalin island are generated by ice rafting (ice hummocks). High dynamics of the ice cover, high concentration and significant ice strength make concrete abrasion depth within the ice zone a critical problem causing demands for exclusive standards for off-shore concrete.

A model of ice-structure interaction has been proposed [21, 27] which allows determining the following parameters of mechanical interaction between ice cover and a structure: number of load cycles, time of penetration of structure into ice sheet, depth of penetration, and regime of ice load to structure. The design cases include phenomena of flow of ice features around the structure. This flow is mainly controlled by the structure-ice friction conditions. The abrasion process of concrete is assumed to depend on the sliding speed and the normal pressure in the contact area. For a specific concrete quality, experiments are performed on the ice concrete contact with cyclic friction wear tests and topographic measurements of abrasion.
A probabilistic simulation model of ice-structure interaction was developed based on numerical modeling of ice load distribution functions and simulation of all probable situations encountered with the actual combinations of input parameter values. For each particular situation the ice load is calculated using a recently developed model of mechanical interaction process between the ice field and marine hydraulic structure [21, 28, 29]. Probable characteristics of ice load, contact stress, mechanical effect path, the structure's material abrasion path and depth were determined

by Monte-Carlo simulations and imitation of all probable situations throughout the entire period of the life time. The following assumptions were made and adopted to the simulation model:

1. The sheet ice is an aggregation of ice formations equally distributed throughout the water area and characterized by the following parameters: thickness h, drift velocity for each direction V, diameter $D_k$, temperature T, concentration N;

2. Ice sheet parameters are independent random values and are shown as monthly distribution histograms based on long-term observations in the particular offshore area;

3. The duration of the design situation is calculated by eq.(1):

$$t_k = P(V_k) \cdot P(D_k) \cdot P(h_k) \cdot P(T_k) \cdot P(N_k) \cdot P(Z_k) \cdot t \tag{1}$$

$P(V_k)$, $P(D_k)$, $P(h_k)$, $P(T_k)$, $P(N_k)$, $P(Z_k)$ are occurrence probabilities of input parameters: ice drift velocity, ice sheet dimensions, thickness and temperature, concentration and sea level fluctuations respectively; $t_k$ is design month of ice season and t is time.

4. Duration of the design situation decreases subject to probability of ice collision with the structure

$$t_c = t_k \cdot \frac{N}{10 \cdot D_k^2} (D_k + D) \cdot (L_0 + D) P(Z_k) \tag{2}$$

where D is diameter of the structure; $L_0$ is initial spacing between ice formations.

For proper calculation of ice loads, three basic groups of probable effects of drifting ice upon the parts of a structure are specified depending on dimensions of the ice formations:
– broken ice with dimensions up to ($D_k \leq 4D$);
– ice floes with dimensions up to (4 $D < D_k \leq 500$ m);
– ice fields ($D_k > 500$ m).

Typical cases of ice-structure interaction are as follows:
**B.** Penetration of structures into the ice field;
**B.1** Penetration of the ice block, slowdown before the structure;
**B.2** Penetration of the ice block with subsequent acceleration caused by another ice floe impact impulse;
**B.3** Penetration of the ice block and shear of ice floe adjacent to structure;
**C.** Stand-still of the ice field in front of the structure;
**C.1** Stand-still of the ice block and velocity slowdown;
**C.2** Stand-still of the ice block with subsequent moving-off caused by another ice floe impact impulse;
**D.** Ice block buckling failure;
**E.** Open water in front of the structure.

The calculation is primarily complicated by determination of time and path of ice-structure interaction. For the purpose of calculation, the law of momentum conservation and the principle of ice field's energy are applied.

The case **B** describes the centric and completely inelastic impact, where all kinetic energy is equated to work of the contact force on structure along the ice penetration path.

$$\int_0^x F_i \Delta x_i = \frac{M_{i+1} \cdot V_{i+1}^2}{2} - \frac{M_i \cdot V_i^2}{2} \tag{3}$$

where $M_i$ is weight of the ice floe at i-th phase; $M_{i+1}$ is weight of the ice floe at next phase; $V_i$ - drift speed at i-th phase; $V_{i+1}$ is drift speed at next phase; $F_i$ is ice force; $\Delta x_i$ is path of mechanical interaction at i-th phase of a particular situation, m.

Current velocity is assumed equal to ice drifting velocity, i.e. $v_w = v_k$, while dependency of ice penetration velocity variation subject to current force can be formulated as

$$V_{i+1} = \sqrt{\frac{M_{i+1} \cdot V_{i+1}^2 + 2(F_i - F_w) \cdot V_i \cdot \Delta t}{M_{i+1}}} \qquad (4)$$

Once the kinetic energy of the ice field is nullified, the ice field will stand still, therefore ice block penetration velocity $V_i = 0$.

The penetration process may be re-commenced once the subsequent ice floes impact the ice block standing still towards the structure (cases **B.2** and **C.2**) with subsequent momentum transfer. As per the law of momentum conservation, the system's total momentum is constant regardless of any internal processes. In turn, the total momentum of the whole system (ice block) can be calculated by summarizing momentums of all ice floes it is composed of. Then the ice block penetration velocity can be calculated as

$$V_{i+1} = \frac{M_i V_i + M_0 V_k}{M_i + M_0} \qquad (5)$$

The ice drift scenario subject to interaction assumed within the simulation model is as follows. Initial contact will be that of either aforesaid cases (**B, C, D, E**). Should the kinetic energy of ice floe be sufficient for penetration, it is penetrated by the structure upon impact (**B.1, B.2**), penetrated and stopped (**C**) or penetrated by the structure and broken apart (**B.3**). Therewith, the ice floe penetration velocity decreases from a certain value $V_0 = V_k$. Upon the first contact, the ice block may either stand still before the structure (**C**), or continue drifting provided that kinetic energy is sufficient (**B.1**), or continue drifting with increased velocity being accelerated by another ice floe impact impulse (**B.2**). Should one (**C.1**) or several ice fields stand still, concentration of ice floes will take place. In this case, each subsequent ice floe will transfer its impulse to the ice block standing still in front of the structure, which may cause the penetration process to re-commence once the kinetic energy of impact impulse is sufficient to move the ice block in front of the structure. Then the ice block penetration velocity can be calculated by eq. (5). Once the ice blocks have stopped and load has been released (**C**), the cycle will repeat upon arrival of new ice floes. In case of ice field shear (**B.3**) the distance between the structure and the first ice floe of the block (**E** – open water) will be calculated as per the following. Calculation continues unless the estimated time t is equal to design situation time $t_c$ subject to collision probability between ice and structure.

Calculations were made with the «IceStrIn» software [21, 29] giving the distribution of probabilistic features of the ice abrasion process for the North-Eastern shelf of the Sakhalin island, see the histogram of ice fields contact pressure distribution in Figure 3. It shows ice load for various ice fractures (ice field brittle fracture force $F_{bp}$; ice field standstill force $F_{cp}$; buckling failure force $F_{bu}$; broken ice force $F_{rb}$).
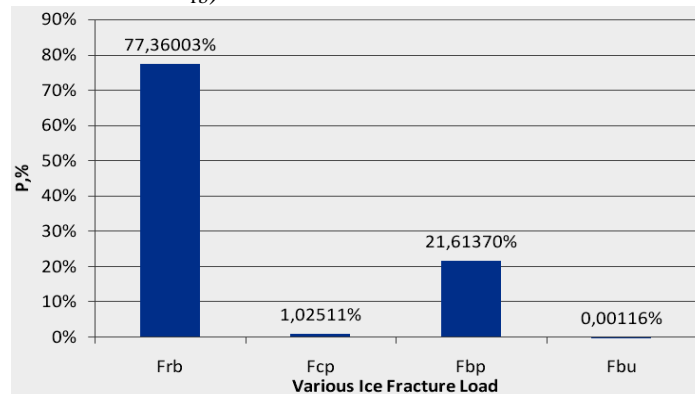


*Figure 3 – Typical histogram of ice load distribution for south western Sea of Okhotsk*

The suggested model is purposed to identify the following parameters of mechanical interaction between sheet ice and hydraulic structure: number of load cycles, time of penetration, length of

penetration way and load regime for the structure. Numerical modeling enables determination of time dependence for the above-mentioned parameters, which may be used to obtain the dynamic characteristics of the ice-structure interaction process, to calculate the fatigue strength of particular structural elements and/or to identify the depth of ice abrasion. Evaluation of the contact pressure and abrasion path length requires an appropriate mathematical tool. The length of the abrasion path is determined by the process of ice formations drift and interaction with the structure.  Up to now, no theoretical models specifying material resistance to ice abrasion have been available. Experimental studies of various materials in terms of resistance to ice abrasion have led to determination of empirical dependence of ice abrasion intensity. Calculation of abrasion shall make allowance both for ice effect on the structure and abrasion resistance of the particular material. The joint use of theoretical model of interaction and empirical model of material deterioration has made it possible to develop a method of ice abrasion depth calculation.

**Ice abrasion laboratory testing and modeling**

Results from concrete ice abrasion tests (both samples taken from structures exposed to ice abrasion and new laboratory concrete)  have been applied to a mathematical model partly based on the above ice sheet movement modeling to provide more reliable abrasion prediction. Concrete samples designed for presumable structure maintenance have also been obtained. The primary test conditions controlled on concrete samples in the ice abrasion test process are contact pressure, ice and air temperature. These are recorded as digital code in real time mode during test by force and temperature sensors. Measurements are made of abrasion depth and pathway (relative concrete-ice displacement for the test duration). These test conditions and observations are introduced in the model as numerical series, processed for further analysis. The file processing order is as follows:
a) analysis of measurements and screening of data, measured prior of after load detaching, i.e. prior to or after completion of experiment. This analysis is made by using test logs, incorporating records of abrasion tests process;
b) determination of average load value in the course of experiment. Once the test includes several phases, the average load value for each phase shall be determined in particular;
c) determination of average test pressure (assuming the contact area dimensions are known). Abrasion path length is measured automatically by a counter computing the number of abrasion rig test cycles. In this case one way concrete-ice dragging path shall be assumed as one cycle. Figure 4 shows the topography of a tested concrete sample surface measured three times prior and after the abrasion test with 0.05 mm accuracy.  Specific abrasion value is determined by dividing the absolute abrasion value by abrasion path length.
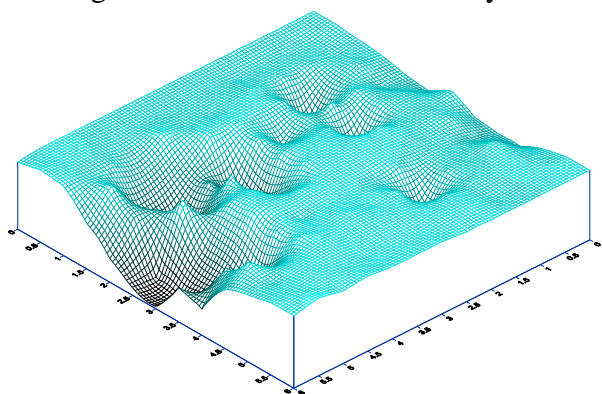


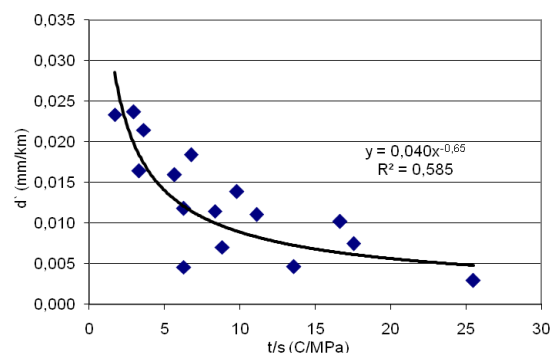Figure 4 - Abrasion test result example

Figure 5 – Coefficient of specific abrasion vs   pressure and temperature for ice zone

$y = 0,040x^{-0,65}$
$R^2 = 0,585$

Figure 5 is based on test results at different pressures and temperatures showing that abrasion

increases with increasing pressure, and that the specific abrasion value decreases as the ice temperature falls. However, under natural conditions it can be assumed that design ice temperature ($-15^0$C) can be met quite rarely due to the thermal effect of seawater and ice cover. Therefore, the abrasion value of the structure will be considerably less affected by temperature compared to the test data obtained within the -5 to $-20^0$C range.
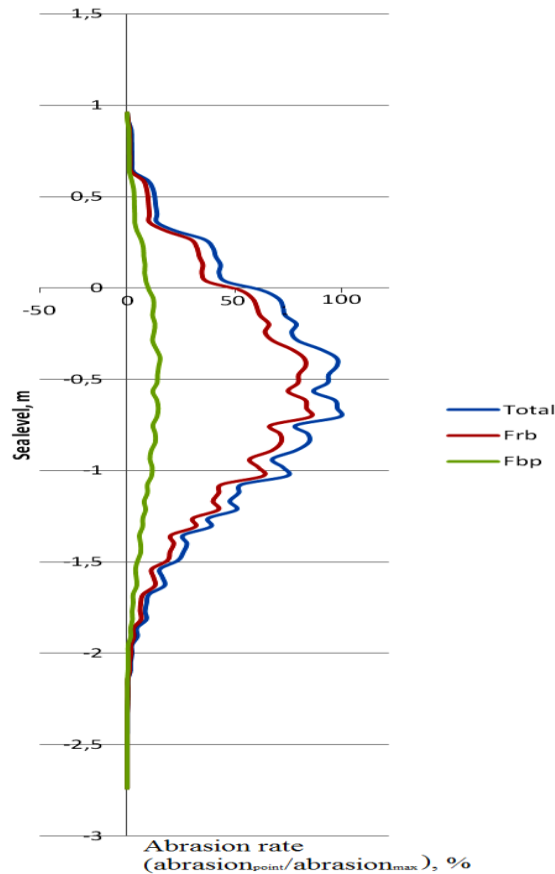


*Figure 6 – Relative concrete ice abrasion variation on concrete in ice zone*

Figure 6 shows diagrams of calculated vertical relative concrete abrasion distribution in the ice zone in the Sea of Okhotsk based on measurements of some concrete types. Ice abrasion tests have been performed at NTNU and FEFU for concrete of various compositions, and concrete abrasion calculations over 40 years in the conditions at Sakhalin island have been made. These results show the possibility of using concrete exposed to the severe ice conditions in the Sea of Okhotsk. Analysis of maximum abrasion value within the ice zone suggests feasibility of building up the required protective concrete layer within the ice zone (Figure 2).

**PORE WATER PRESSURE BY ROUGH CONCRETE SURFACE INDENTED IN ICE**

**Impact and contact pressure**

In the following a hydraulic contact pressure fracture mechanism is introduced to proceed in the concrete material modeling of ice abrasion. The mechanism explains concrete fracture by water being forced into the pore system of the concrete as ice impacts the concrete surface under wet ice-concrete interface conditions. According to contact mechanics the local pressure between two materials can be very high depending on load, surface shape and materials [30, 31]. For elastic contact the relative movement between the materials should be fast enough to reduce time dependant deformations such as creep and plastic flow. For moving ice sheets the velocity at contact can be high enough to cause brittle behaviour [32]. Figure 7 from [33] shows how ice

crystal hardness increases as loading time and temperature reduces, and being larger than 50 MPa at very short contact times down to $10^{-4}$ s and low temperatures.
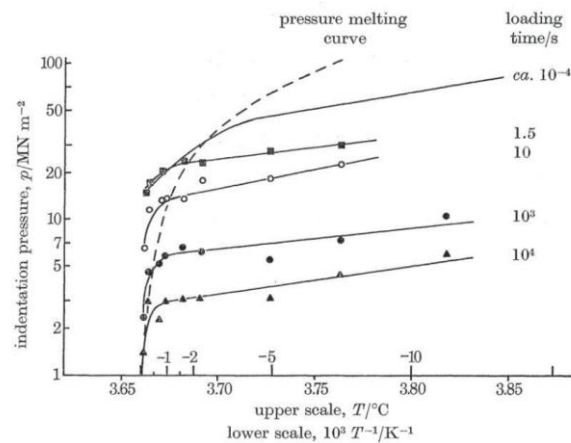


*Figure 7 – Hardness of pure ice crystals at varying indentation times, from Barnes et al [33]*

Furthermore it seems that the stress is approaching and/or limited by the pressure melting curve according to Clausius-Clapeyron's equation (broken line) [33,34]. The resulting local contact pressure and water flow into the concrete surface pores as ice is impacting on a rough concrete surface can be estimated according to contact mechanics [30, 31] and concrete permeability. The local contact can trap and force water into the concrete from sea water surrounding submerged ice, from the Liquid Like Layer (LLL) on ice [34] and from pressurized melting. The importance of wet impact contact for abrasion is supported by observations of higher concrete abrasion on wet than on dry concrete surfaces both with ice [13] and with steel-studded car tires [36]. An estimate of the elastic indentation pressure as ice is forced towards a rough concrete surface over short time can be based on assumptions about surface roughness geometry and elastic properties of ice and concrete see figure 8.
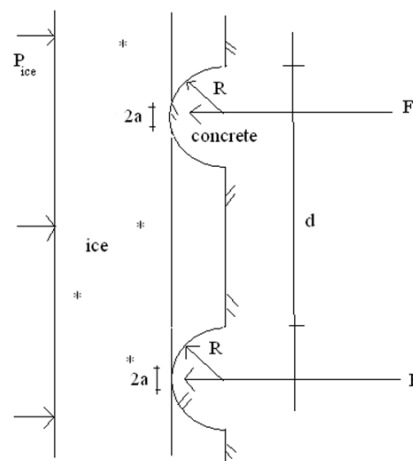


*Figure 8  - Plane ice surface (left) moving with average pressure $P_{ice}$ towards rough concrete surface with microscopic asperities radii R, spacing d, reaction forces F and contact radii a*

Figure 8 shows the simplified local contact zone between a plane ice surface with a mean ice pressure $p_{ice}$ moving towards a rough concrete material surface and water between. The contact is simplified as a combination of concrete half-spheres and plane vertical concrete and ice-surfaces. The reaction forces, F, from each half-sphere and the radii, a, of the contact zones are also drawn. Figure 9 shows a close up of the tip of one asperity and also shows water trapped within the contact zone with diameter 2a in figure 8. Due to uneven surface, water can be trapped in very small pockets at the tips of the concrete asperities. The thin lens-shaped pocket between

ice and concrete in figure 9 is assumed closed around the rim of the asperity so that water cannot escape sideways.
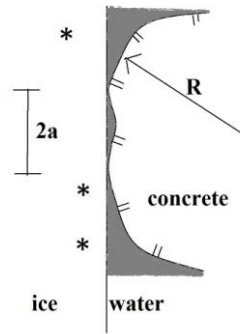


*Figure 9 – Assumed water trapping in contact zone ice/concrete at asperity (R ≈ 0.01 – 10 mm)*

This local trapping of water between ice and roughness in figure 9 could be further illustrated as shown in figure 10. Figure 10 shows a piston-like mechanism where water is trapped in a pocket of concrete acting as cylinder and the ice pushed as a piston into the concrete cylinder. The pressure in the cylinder is limited by the strength of the ice-piston. Once the pressure exerted by the ice on the water in the cylinder exceeds the compressive strength of the ice, the ice crushes. In this way the water pressure is limited by the ice strength, but can be maintained at that level if the ice movement forces more ice into the concrete cylinder. We asume there always are available places for this ice-piston like impact at the tip of the concrete surface asperities.
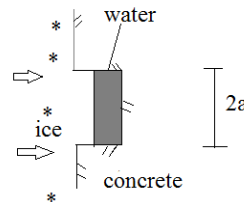


*Figure 10 – Water trapped in cylinder-like concrete chamber where water pressure is limited by strength of ice acting as piston and by permeability of concrete*

The mean contact pressure $p_m$ under the contact zone of radius a is assumed to follow Hertz contact law, and so is 2/3 of the maximum contact pressure $p_o$, eq.(6) [30, 31]:

$$p_m = \frac{2}{3} p_o = \frac{F}{\pi a^2}$$

(6)

We assume that the trapped water is incompressible so that deformation of concrete and ice will force water into the concrete. The ice is effectively impermeable when it has no or very low brine pocket content ($< 5$ vol-%) [37, 38]. The flow can then be assumed only into the concrete. The radius a of the contact surface is then given by the reaction force F, the radius R of the assumed sphere shape and the reduced E-modulus E* eq.(7) [30, 31]:

$$a^3 = \frac{3FR}{4E^*}$$

(7)

The reduced E-modulus E* depends on Poissons ratios $\nu$ and E-modulii of ice and concrete:

$$\frac{1}{E^*} = \frac{1-\nu_i^2}{E_i} + \frac{1-\nu_c^2}{E_c}$$

(8)

The maximum ice contact pressure is assumed equal to the Hertzian contact pressure [30, 31]. The concrete-ice contact radius, a, for the chosen surface roughness radius R can then be

determined from maximum pore water pressure $p_{eff}$ (which is limited by the hardness of the ice) by dividing eq (7) with the single indent contact area $\pi a^2$ giving:

$$a = \frac{3\pi}{4} \frac{R p_{eff}}{E^*}$$

(9)

Material fracture in concrete due to contact pressure may occur as the maximum tensile stress exceeds concrete tensile strength:

$$p_{crit} = f_{c,t} \leq p_{eff} \approx (p_m - p_{ice})$$

(10)

Where $p_{crit}$ [MPa] critical pressure at which fracture of concrete occurs, $f_{c,t}$ [MPa] concrete tensile strength, $p_m$ [MPa] (Hertzian) local contact pressure by concrete indenting ice, eq.(6) $p_{ice}$ [MPa] average ice pressure on surface, $p_{eff}$ [MPa] effective local hydraulic pressure in pore water at concrete surface. We assume that the damage (cracking, spalling) takes place at parts of the asperities shown in Figures 8 and 9 that are close to, to but not in direct contact with the elastic ice-concrete contacts. For elastic indentation of a sphere in a surface (elastic half-space), the maximum values of tensile stress, its position and the local deformation are given in [31, 39]. The position of max tensile stress is usually at the rim of the contact zone (radius = a), but it will be a quite small fraction of the normal contact pressure. The compressive strength of granular ice is of the same order of magnitude as the tensile strength of concrete. Therefore the contact tensile stress in the concrete at the rim of the contact point will be very low compared to when rough concrete indents a harder material than ice. It was shown in [40] that the above equations easily can compute contact stresses larger than ice hardness when a flat ice surface impacts concrete surfaces with half-spheres as shown in Figure 8. The half-spheres in Figure 8 are shown with realistic roughness R= 0.05 – 5 and spacing d≈ 0.1 - 10 mm and ice pressure $p_{ice}$= 1 MPa. However, it seems that hydraulic pore water pressure, which can be transferred directly into tensile stress in the concrete when the pore system is water filled, is a better basis for determination of concrete fracture stress and abrasion than plain contact mechanical stress. Concrete tensile stress from hydraulic pore pressure will be limited by the ice hardness which easily can be higher than concrete tensile strength. Therefore, we suggest that contact mechanics is only used in the calculation of contact area using equation (9), while limiting the contact pressure $p_m$ to the strength or hardness of ice. The arising pore water pressure is then investigated as a cause of tensile fracture during short time brittle impact. During longer loading times [32] the contact pressure will be lower due to ice creep. Finite element modelling [31] shows that for plastic deformation the contact stress $p_m$ reduces largely compared to the elastic case and spreads outside the elastic contact zone with diameter 2a. However, for short time elastic contact the main assumptions of elastic (Hertzian) contact mechanics can apply to the ice-concrete sphere normal contact: large radii of curvature of the contacting bodies compared to the circle of contact, the dimensions of each body are large compared with the circle of contact, and the local contact (i.e. on the sphere with radius R) is frictionless so that only normal pressure is transmitted. The last main assumption: no pressure outside the zone of contact applies during impact when there is little/no creep or plastic flow during short time impacts.

**Hydraulic pore pressure and concrete fracture**

Flow into the concrete due to the contact pressure obeys D'Arcy, which at steady-state in saturated concrete writes:

$$j = -K \frac{dp}{dx}$$

(11)

Where j [m/s]: flow in concrete, K [m/s]: coefficient of permeability of concrete and dp/dx [m/m]: hydraulic pressure gradient. However, in our case the inwards flow is non-steady state.

This flow can be assumed to be a sharp front of water flowing from the indenting pressure at the surface and inwards. The permeability between the surface and the front [41] is assumed constant K ($\neq$ K(T, s)). The contact and indentation of concrete in ice gives the local effective pressure $p_{eff}$ and depth of water penetration, x, during the time of indentation $t_{ind}$. Then the penetration depth $x(t_{ind})$ can be calculated as a non-steady state D'arcy flow according to equation (12) [16, 41]:

$$x(t_{ind})=\sqrt{\frac{2p_{eff}t_{ind}K\cdot10^6}{s\cdot g\cdot\rho_w}}$$

(12)

Where x [m] depth of penetration, $t_{ind}$ [s] indentation time, s [$m^3/m^3$] air pore volume fraction water filled by pressure ($\approx$ 0.02–0.06 [16]), g = 9.81 $m/s^2$, $\rho_w$ = 1000 $kg/m^3$. The fraction s = 0 corresponds to a saturated capillary and gel pore system and empty air voids. The air voids stay empty during suction but then fill during pressure saturation. Figure 11 shows variation of depth of penetration, x, with concrete permeability, K, and time of indentation, $t_{ind}$ for effective hydraulic pressure 30 MPa. This is chosen as a conservative value of ice crystal strength at short time. The air pore volume fraction s filled by pressure is assumed to be 0.06.

Figure 11 shows that for this high contact pressure, which is realistic during short time, the calculated penetration depth is very low for indentation times 0.01 - 1 s (figure 7) and below. It is less than 10 - 100 microns for the two chosen very low permeability-values representing rock and high-performance concrete. The exact permeability is difficult to estimate as ice formation can reduce the concrete permeability further [42, 43].
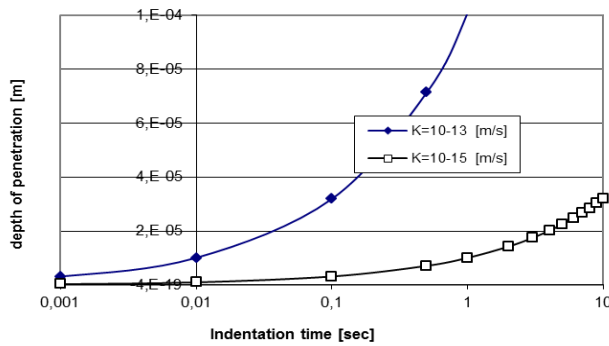


*Figure 11 - Depth of penetration as function of indentation time at 30 MPa contact pressure*

A good air void system with an air void spacing factor of, say 200 microns (=0.2 mm, will not be able to protect against this kind of hydraulic pressure even though it protects concrete from frost damage [5,44]. Furthermore, the transport time is so short that there will be no time for relaxation of the local pore water pressure in a thin concrete surface layer [45]. Neither will there be any time for ice-creep since the ice relaxation rate is at a minimum and the E-modulus of the ice at maximum at high strain rates [32]. Therefore high hydraulic pore pressure and fracture can occur. A further poromechanics analysis could elucidate this.

The pore pressure can simplified be assumed to drop linearly with depth from $p_{eff}$ at the concrete surface to a lower pressure at the front of the water penetration $x(t_{ind})$. At the depth $x(t_{ind})$ the pressure is assumed to be atmospheric. It can even be lower according to the Kelvin equation if the degree of saturation is sufficiently low beyond the penetrating front. During short time the linear inwards pressure gradient then is -($p_{eff}/x(t_{ind})$). That is, concrete damage will arise in a thin layer of surface concrete as the water pressure exceeds the concrete tensile strength $f_{t,c}$. This can happen at the tip of concrete surface asperities, continuously creating new fractured surface. The depth where this critical pressure $p_{crit}$, occurs is termed critical depth, $x_{crit}$. $x_{crit}$ can be determined from the assumed linear pressure distribution. The pressure drop from the surface then is:

$$p(x) = p_{eff} - \frac{p_{eff}}{x(t_{ind})} \cdot x \tag{13}$$

With $p(x)$ = hydraulic pore pressure at depth x below concrete surface. Solving for the critical depth $x_{crit}$, from the fracture criterion $p(x) = f_{t,c} < p_{eff}$ this gives:

$$x_{crit} = x(t_{ind})[1 - \frac{f_{c,t}}{p_{eff}}] \tag{14}$$

Where $x(t_{ind})$ is given by eq. (12). Eq.(14) predicts that the fracture depth will be a fraction of the maximum water penetration depth, depending on concrete tensile strength and effective local pressure at the concrete surface asperity. The concrete tensile strength in eq. (14) rarely exceeds 8 MPa whereas the effective pressure in the piston on figures 9 and 10 is set at 30 MPa giving critical depth = 22/30 of the water penetration at impact. This is considered a realistic value based on the discussion with figure 7. The shape and size of the fracture is not known though likely to have some inclination to the surface plane. The fractured material will thus have some geometry (cylinder, cone etc) that can be estimated from the contact radius in eq. (9) and the critical pressure depth in eq. (14). From a simplified ice sheet drift, indentation and fracturing process with cylindrical fracture shape ($x_{crit} a^2\pi$), the analytical equation (15) was proposed for ice abrasion for indents caused by impact only [46]:

$$ABR_c = \frac{L_{ice,ann}}{D_{fragment}} \cdot \frac{x_{crit} \cdot \left(\frac{\sqrt{A_s}}{d} + 1\right)^2 \cdot a^2 \pi \cdot 1000}{A_s} \tag{15}$$

Where $ABR_c$ [mm/yr] is ice abrasion, $L_{ice,ann}$ [m/yr] is ice movement, $D_{fragment}$ [m] is size of ice fragment after impact and crushing [11,46], d [m] is length between individual indentation points in square grid (see figure 8), $x_{crit}$: eq.(14), a: eq.(9) and $A_s$ [m²] is concrete surface area exposed to ice (1m²). Table 1 shows the abrasion calculation with eq.(15) compared to observations of ice abrasion on the Canadian Confederation Bridge [15] and a Finnish lighthouse [1].

*Table 1 - Impact ice abrasion calculation compared with observations on concrete structures*

| Structure | K, $f_t$, d, R, E*, $D_{fragm}$, $L_{ice}$ (km/yr), $t_{ind}$, $p_{eff}$ | Measured (mm/yr) | Calc. (eq.15) (mm/yr) |
|---|---|---|---|
| Confederation bridge [15] | $\approx 10^{-13}$,7,0.01, 0.01,8197,0.25,25,0.1,22.5 | $\approx 0,3$ | 0,3 |
| Finnish Lighthouse [1] | $\approx 10^{-11}$,5,0.025,0.0125,7891,0.25,25,0.1,22.5 | $\approx 1$ | 1,0 |

Table 1 is based on deterministic values of the parameters in the above equations. To estimate these values is particularly difficult for the ice load parameters. The estimates in table 1 are based on existing meteorological data for the Baltic Sea and the Sea of Okhotsk and assuming that the ice drift at the Confederation Bridge is similar to at the Baltic Sea lighthouse. One main simplification of the ice load is to assume that 1000 km/40 years = 25 km/year represents the ice load in a point on the concrete surface. This "grand average" will vary both over height, structure circumference as well as due to ice conditions (thickness, concentration, drift direction etc). The results of table 2 show that the model can predict realistic impact ice abrasion for these two different field exposed concretes based on the estimated ice data and concrete material data.

Table 2 shows that this approach can also be used to calculate sliding abrasion as scratching by introducing friction between ice and concrete, $\mu_{i-c}$, in eq.(12) to give scratching pressure by equation (16). The very short indentation time is then switched with the longer sliding time, $t_{slide}$, which is assumed to be a series of elastic indents. The water under pressure is assumed to be between the tip of the scratch and the concrete surface asperity scratching the ice. The abrasion

depth is again given by eq.(15) setting the number of impacts (L/D) = 1 and using $x(t)_{slide}$ from (eq.16) in eq.(14) instead of $x(t)_{ind}$ from eq.(12).

$$x\left(t\right)_{slide} = \sqrt{\frac{2\mu_{i-c} \cdot p_m \cdot t_{slide} \cdot K \cdot 10^6}{s \cdot g \cdot \rho_w}} \tag{16}$$

*Table 2 – Sliding ice abrasion calculation compared with values observed in lab tests*

| Parameters | Observed | Calculated |
|---|---|---|
| $K, f_t, d, R, E^*, t_{slide}, p_{eff}$ | (mm/km) | (mm/km) |
| 5.10-11, 4, 0.001, 0.004, 5132, 100800, 22.5 | ≈0.1 - 20 | ≈1.5 |

The abrasion calculated in this simplified way agrees with typical sliding abrasion values observed in laboratory tests [12]. The model can also give simple concrete strength vs ice movement relations to abrasion like [1]. The model is, however, quite sensitive to several of the parameters. The effective pressure has for example been adjusted to 22.5 MPa to obtain the right abrasion and obviously there are infinite numbers of variations of indentation time, permeability and surface roughness that can give any desired abrasion.

The contact area of the impacts and scratches leading to concrete ice abrasion can also be estimated by performing a numerical simulation as shown in figure 6 for all points on the concrete surface. This can be done assuming that all contacts in the simulation have effective contact pressure equal to ice crystal hardness. This, however, leads to a very high abrasion; approximately 680 times higher than the maximum abrasion value in the tidal zone estimated for 40 years shown in figure 6. Thus, if the rough concrete-ice crystal indentation is responsible for the total ice abrasion at such an effective point contact pressure, it would be a model with a random and discontinuous process. With the assumed concrete roughness and ice-contact model then only a very small fraction of the real number of concrete-ice contacts cause abrasion; in the order of (1/680) = 0,15 %. It thus appears that more research is needed to proceed in the modelling of concrete ice abrasion as has already been emphasized [47-49]. This should include both the aforementioned poromechanical analysis adapted to external ice indenting concrete [50,51] as well as advanced analysis of the stress at the contact surfaces and the liquid flow between ice and concrete [52,53].

**CONCLUSIONS**

To proceed in the development of prediction tools for ice abrasion on concrete structures, mechanisms possibly causing this kind of damage have been reviewed. Then we applied a comprehensive prediction tool for concrete ice abrasion in arctic and sub-arctic areas developed at FEFU. The tool is based on field and laboratory measurements of ice abrasion, ice drift in the Sea of Okhotsk offshore and impact force modelling on structures. Probabilistic computations of the abrasion in every point of the structure are based on ice impact force, ice drift model and field- and laboratory measurements of concrete ice abrasion. The predicted ice abrasion is used to design concrete that can stand very severe ice abrasion conditions. Simulations were made with maximum pressure equal to hardness of ice crystals. This was done to simulate hydraulic pore pressure in concrete arising from contact stress by ice impact and scratching with water in the interface between ice and the rough concrete surface. A maximum attainable contact pressure equal to hardness of pure ice crystals was applied in the numerical simulation model that calculates ice abrasion in every point on the surface of the structure. The simulations showed that if hydraulic pore pressure causes abrasion this will happen in only 0.15% of the point impacts.

## ACKNOWLEDGEMENTS

## REFERENCES

1.   Huovinen S. (1993) Abrasion of concrete structures by ice, Cem Con Res 23 (1) 69-82.
2.   Huovinen S. (1990) Doctoral thesis VTT Publications 62, Finland, 110 p, app. 31 p.
3.   Vølund L. et al. (2003) Ice loads on offshore wind turbine foundations – final report, Carl Bro, El-kraft System, Energi E2 DOCS #15822, Denmark, 12 p.
4.   Powers T.C. (1945) PCA Bull. 5 245-271, Terzhaghi R., Bull.5A (1946) 272-1 – 272-20
5.   Powers T.C. (1949) Proceedings Highway Research Board 29,184-211
6.   Helmuth R.A.(1960) Proc 4th Int Symp. Chem Cem VII, Nat. Bur of Standards, 855-869
7.   Jacobsen S. (2002) Frost damage in concrete, Rilem proc. PRO25 pp.41-51
8.   Valenza J.J., Scherer G.W. (2007) Materials and Structures V40, N3, 259-268.
9.   Sun Z, Scherer G.W (2010) Cement and Concrete Research V40, N2, 260-270.
10.  Sodhi D.S. (2008) Nordic Concrete Federation Worksh. Proceed. ISSN 0800-6377, 35-44
11.  Timco G.W., Frederking G.W. (1993) Cold Reg Sci and Tech (22) 77-97.
12.  Møen E., Jacobsen S., Myra H. (2008) ref as [10] pp.59-103.
13.  Jansson J.E. (1988) Proc 7th Int Conf Offsh Mech Arct.Eng, Am S Mech Eng V3 225-231.
14.  Hara F., Saeki H., Sato M, Takahasi Y., Tachibana H. (1995) Concrete under severe conditions, Consec'95, Sapporo, E&FN Spon, V1, 485-494.
15.  Newhook J.P, McGuinn D.J. (2007) Confederation Bridge Engineering Summit 1997-2007 Proceedings Canadian Society for Civil Engineering, 145-157.
16.  Neville A.M. (1995) Properties of concrete, 4th ed., Pearson Prentice Hall, p. 495.
17.  Sistonen E., Leivo M., Puttonen J.(2008) ref as [10], 5-15.
18.  Kayaba T., Kato K., Hokkirigawa K. (1983, 1984) Wear (87) 151-161 (96) 255-265
19.  Fosså K.T. (2008) Improvement of the ice zone on sub-arctic structures, ref as [10] 1-4
20.  Wood, R.J.K. (2009) University of Southampton personal communication August 28
21.  Bekker A.T., Uvarova T.E., Kim S.D.(2003) Abrasion Effect of Ice Cover on Supports of Hydraulic Engineering Structures in Conditions of Sakhalin island Shelf // Proc. Int. Offshore and Polar Engineering Conf., Honolulu, 230-235.
22.  Blackwelder E.(1940) The hardness of ice, Am. J of Sc V38 N1, 61-62.
23.  Offenbacher E.L., Roselmann I.C. (1971) Nature, Physical Sciences V.234, 112-113.
24.  Ackley AF (1973) Symp on Chem and Phys of Ice, Royal Soc of Canada XIII, 382-386.
25.  Khrapatyi N.G. (1981) Dynamic ice interaction for hydraulic marine structures on continental shelf, Ch.VI. Methods for determination of hardness of ice and selection of ice strength, Dr. Sc. Thesis, Far Eastern Polytechnic Inst., p.252.
26.  Wang X.H., Jacobsen S., He J.Y., Zhang Z., Lee S.F., Lein H.L. (2009) Cement and Concrete Research V39, N8, 701-715.
27.  Bekker A.T. (2008) Problems of the ice cover abrading action on legs of concrete offshore structures, ref. as [10] 45-58.
28.  Bekker A.T., Jacobsen S., Uvarova T.E., Pomnikov E.E., Kim L.V. (2011) Evaluation of danger from ice abrasion of offshore platforms in Far Eastern seas, Proc. RAO/CIS Offshore conference, St-Petersburg, 262-265.

29. Bekker A.T., Uvarova T.E., Pomnikov E.E. (2011) Calculation of ice abrasion for the lighthouses installed in the gulf of Bothnia, Proc. Int Conf on Port and Ocean Engineering under Arctic Conditions, July 10-14, 2011, Montréal, Canada, 155-160.

30. Hertz H. (1881) Journal of Pure and Applied Math. 92, 156-171 (in German).

31. Fischer-Cripps A.C. (2007) Introduction to Contact Mechanics, Springer p.101.

32. Schulson E.M, Duval P.(2009) Creep and Fracture of Ice, Cambridge Univ- Press, 401 p.

33. Barnes P., Tabor D., Walker J.C.F (1971) The friction and creep of polycrystalline ice, Proc. Royal Soc. London A Vol.324 No.1557 pp.127-155

34. Hobbs P.V. (1974) Ice Physics, Clarendon Press, Oxford. P.392

35. Barnes P., Tabor D. (1966) Plastic flow and pressure melting in the deformation of Ice I, Nature V210, 878-882.

36. Gjørv O. E., Bærland T., Rønning H.R.(1987) HS concrete for highway pavements and bridge decks, Proc 1st Int Symp Utiliz HSC. Ed. Holand I et al, TAPIR, Norway 111-122

37. Pringle D. Miner J. Eicken H. Golden K. (2009) J Geophys. Res V.114, C12017, 14 p.

38. Golden K. Eicken H. Heaton A. Miner J. Pringle D Zhu (2007) Geophys. Res Letters V.34, L16501, 6 p.

39. Sneddon I.N. (1965) The relation between load and penetration in the axisymmetric Boussinesq problem for a punch of arbitrary profile, Int.J. of Eng Sci., V3, 47-57.

40. Jacobsen S. (2010) Proc Nord. Minisem. ISBN 978-82-8208-020-0 No. Con. Fed.109-122.

41. Hoff W. D. Hall C. (2002) Spon press London and New York, 318 p.

42. Hanaor A.(1982) Magazine of Conc Res 34 (20) 155-162.

43. Fagerlund G. (1992) Nordic Concrete Research Publ. 1/1992 (No.11) 20-36.

44. Pigeon M., Pleau R.(1995) Durability of concrete in cold climates, E&FN Spon, London

45. Vichit-Vadakan W., Scherer G.W. (2003) Cement and Concrete Research, 33, 1925-1932.

46. Jacobsen S. (2011) Nordic Conc. Res. Publ. No 43, ISBN 978-82-8208-025-3, ISSN 0800-6377, pp.163-166

47. Jacobsen S., Sistonen E., Huovinen S., Marchand J., Tremblay M-H. (2007) Ice abrasion, frost, deicer salt scaling and reinforcement corrosion on concrete structures: interaction and service Life, CONSEC'07, France, LCPC, Ed. F.Toutlemonde et.al 1137-1152

48. Jacobsen S., Sistonen E., Huovinen S., Marchand J., Tremblay M-H.(2006) Abrasion and scaling of concrete by ice, studded tires and frost salt: interaction and service life modelling, 2nd Int Symp Adv in Concr through Sc & Eng, Quebec RILEM Proc 51, 23 p.'

49. Sistonen E., Jacobsen S.(2008) Probabilistic service life modelling of ice abrasion on concrete structures, ref. as [10] pp.138-145

50. Scherer G. (2011) Poromechanics of frost damage, in "Mechanics and Physics of Porous Solids (MPPS) - A tribute to Prof. Olivier Coussy", 15 p.

51. Coussy O., Monteiro P.(2008,2009) "Poroelastic model of concrete to freezing temperature", C&CR 38, pp.40-48, Errata to "Poroelastic model….", C&CR39, pp.371-372

52. Yastrebov V.A, Durand J., Proudhon H., Cailletaud G.(2011) Rough surface contact analysis by means of the Finite Element Method and of a new reduced model, Comptes Rendus Mecanique 339, pp.473-490

53. Cailletaud G. (2012) Guest lecture at NTNU/Dept of Structural Engineering, personal communication